Natural Hazards (2020) 103:1479–1497
https://doi.org/10.1007/s11069-020-04046-0

ORIGINAL PAPER

Study on the creep behaviours and the improved Burgers model of a loess landslide considering matric suction

Zhilu Chang[1] · Huanxiang Gao[2] · Faming Huang[1] · Jiawu Chen[1] · Jinsong Huang[3] · Zizheng Guo[4]

Received: 27 February 2020 / Accepted: 4 May 2020 / Published online: 15 May 2020

Abstract

Loess landslides frequently occur in the northwest area of China, leading to serious damage to the society and economy. Under the effects of rainfall and groundwater seepage, the stress–strain behaviours of Malan loess landslides are closely related to the saturated–unsaturated state of slide mass. Hence, it is of great significance to study the creep behaviours of Malan loess considering matric suction. First, the sliding-zone soil of a typical Malan loess landslide is collected to carry out tri-axial creep tests with a confining pressure of 100 kPa and diffident matric suction values of 20, 50 and 80 kPa. Then, a stress–suction–strain–time model (an improved Burgers model) is established by connecting a nonlinear dashpot element in series with the Burgers model and combining this with the functional relationship between the viscoelastic modulus and matric suction. The results show that (1) the Malan loess has obvious creep behaviours with viscoelastic and viscoplastic creep properties, (2) the long-term shear strength of Malan loess increases along with the increase in its matric suction, and (3) the improved Burgers model can more accurately describe the unsaturated creep behaviours of Malan loess with matric suction compared to the traditional Burgers model.

Keywords Malan loess landslide · Matric suction · Creep behaviours · Tri-axial creep test · Improved burger model

✉ Faming Huang
faminghuang@ncu.edu.cn

[1] School of Civil Engineering and Architecture, Nanchang University, Nanchang 330031, China

[2] School of Qianhu, Nanchang University, Nanchang 330031, China

[3] Discipline of Civil, Surveying and Environmental Engineering, Priority Research Centre for Geotechnical Science and Engineering, University of Newcastle, Newcastle, NSW, Australia

[4] Faculty of Engineering, China University of Geosciences, Wuhan 430074, China

1 Introduction

Loess, formed in the Quaternary period, is a kind of sediment with features of multiple interspaces and weak cementation. The total distribution area of loess in the northwest and north China reaches 6.3×10^5 km^2 (Xu et al. 2017). In recent years, loess landslides have frequently occurred in these areas due to extreme weather conditions and unreasonable human engineering constructions, which seriously threaten local people's safety and property. Therefore, it is of great significance to study the instability mechanism of loess landslides.

Recently, loess landslides have attracted the attention of many scholars. Related literatures indicate that the evolution and occurrence of loess landslides are affected by the combining actions of various internal and external factors, including the physical and mechanical properties of loess, slope structure, earthquake, rainfall, changes of slope groundwater level, human engineering activities, etc. (Fan et al. 2017; Hou et al. 2018; Huang et al. 2017; Lee et al. 2014; Ling et al. 2014; Wang et al. 2013; Xu et al. 2014; Zhang and Wang 2007; Zhuang et al. 2018). Among these factors, the physical and mechanical properties of loess can be characterized as loose structure, high clay mineral content, water sensitivity, collapsibility and sensitivity to matric suction. These special physical and mechanical properties offer material conditions for the occurrence of loess landslides (Chen et al. 2012; Qiu et al. 2018; Xu et al. 2018; Zhang and Liu 2009). In addition, physical and mechanical properties of loess readily change under heavy rainfall and contribute to the instability of loess slopes. Moreover, landslides can be regarded as a process where stress and strain of sliding mass are continuously adjusted over time under the action of gravity and external forces (Bhat et al. 2013; Zhou et al. 2012). Therefore, it is necessary to study the variations of physical and mechanical properties of loess under various conditions and further explore the creep behaviours of loess slope corresponding to these variations to reveal the deformation and failure mechanism of loess landslides.

It is known that some landslides occurred due to the creep behaviours of soil slope (Lai et al. 2010). Over the past decades, researchers have conducted numerous studies to investigate the creep behaviours of the soil slope and mainly focused on the following aspects. On one hand, in order to investigate the deformation and strength features of sliding-zone soil, the creep behaviours have been studied by a series of laboratory experiments considering different confining pressures, water contents, stress levels, etc. (Xie et al. 2018; Yang et al. 2010; Zhao and Zhou 2013). On the other hand, the creep models of soil slope are put forward based on the results of tri-axial creep tests and theoretical analysis (Li et al. 2011). Literature review indicates that there are mainly four types of creep models, namely the Cam–Clay model, Duncan–Chang model, Kelvin model and Burgers model, that are widely accepted and applied by researchers at present (Graham et al. 2001; Huang et al. 2009; Liu and Carter 2002; Nguyen et al. 2011; Wan et al. 2011). In addition, the creep models are mainly built based on the empirical, element, yield surface and/or damage effect modelling patterns (Sivasithamparam et al. 2015; Wang and Qiao 2011). Among those creep models, the Burgers model is widely used to describe creep behaviours of various rocks and soils due to its advantages of intuitive concept, clear physical meanings of parameters and simple calculations (Zhao et al. 2009). Hence, the Burgers model is also selected to explore the creep behaviours of loess landslides in this study.

Matric suction plays an important role in the creep process of loess landslides (Song et al. 2016). This is because the matric suction, which can be defined as the difference value between gas pressure and water pressure, is a critical parameter to

describe the mechanical properties of unsaturated soil. Furthermore, loess landslides are in the unsaturated state due to the influences of rainfall and changes of groundwater level; the stability of the loess slope is closely related to the saturated and/or unsaturated state. The current studies mainly focus on the relationships between matric suction and the mechanical properties of unsaturated soil (Fredlund et al. 1995; Gallage and Uchimura 2016; Mahmood et al. 2016) as well as the influences of matric suction in the landslide failure mechanism, monitoring and warning (Jeong et al. 2017; Tang et al. 2014; Yuliza et al. 2016). However, there are few studies focusing on the creep behaviours of loess landslides under the action of matric suction. Only Lai et al. (2012) have used the sliding-zone soil of a landslide in the Three Gorges region to carry out unsaturated tri-axial creep tests under conditions of different matric suction values and different deviatoric stress levels and then established the corresponding stress–suction–strain–time model. Zhu and Yu (2014) proposed an improved Mesri creep model involving stress–matric suction–strain–time, which is more precise than the Mesri creep model in predicting the unsaturated creep behaviours of weak intercalated soils. Hence, it is necessary to study the creep behaviours of loess landslides under the action of matric suction.

In this study, Malan loess collected from the Loess Plateau area of China is selected to conduct tri-axial creep tests under control conditions of different matric suction values with a GDS experimental instrument. The relationships between stress–strain and experimental times under different matric suctions and stress loading levels are studied. In addition, the long-term strength changes of Malan loess soil samples under different matric suctions are analysed. Furthermore, an improved Burgers creep model is established by considering the influence of matric suction on the Burgers model and the creep behaviours in the acceleration creep stage, because the traditional Burgers model has not considering the effects of matrix suction and acceleration creep behaviours of Malan loess. These studies can provide experimental experience and theoretical guidance for revealing the creep mechanical properties of an unsaturated loess slope.

2 Materials and methods

2.1 Experimental material

Malan loess (Q_{p3}^{eol}), which is collected from the sliding-zone soil of loess landslide where located in Lingbao City of Henan province, China, is selected as the sample soil. The basic physical and mechanical properties of the sample soil are shown in Table 1. It can be seen from Table 1 that the specific gravity is 2.69 by specific gravity tests, the saturation hydraulic conductivity is tested to 1.26×10^{-6} m/s, and the maximum dry density is 1.80 g/cm^3 as well as the optimum moisture content is 17.35%. The particle distribution curves of the sample soil indicate that its compositions include sand (0.075–2 mm), silt (0.005–0.075 mm) and clay (< 0.005 mm) with percentages of 4.50%, 84.04% and 11.47%, respectively (Fig. 1). Moreover, the main mineral components of the sample soil include quartz (54.66%), feldspar (15.05%), calcite (12.40%), illite (8.97%), chlorite (7.20%) and dolomite (1.55%) based on X-ray diffraction (XRD) experiments (Fig. 2).

Table 1 The basic physical and mechanical parameters of Malan loess

Specific gravity	Liquid limit	Plastic limit	Void	Saturation hydraulic conductivity Ks(m/s)	Maximum dry density (g/cm^3)	Optimum moisture content (%)
2.69	29.87	15.33	0.672	1.26×10^{-6}	1.796	17.35

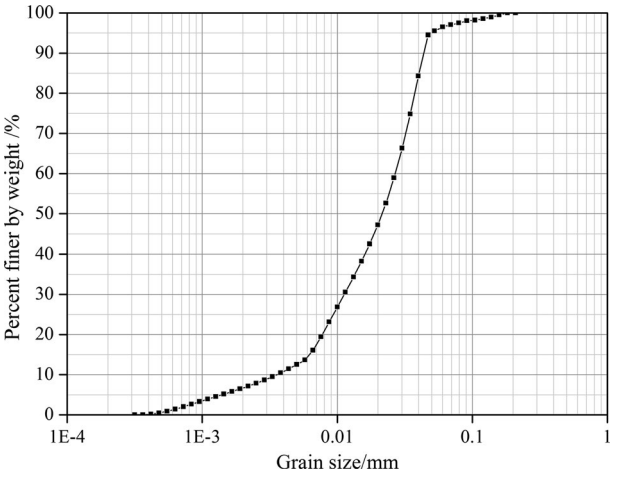

Fig. 1 Particle size distributions of the Malan loess

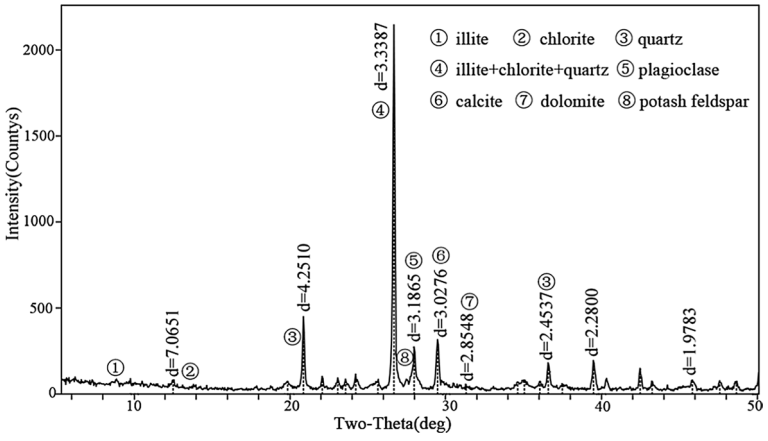

Fig. 2 XRD pattern of Malan loess

2.2 Experimental schemes

The GDS tri-axial instrument of unsaturated soil is adopted in this study. This instrument mainly includes four parts: the confining pressure control device, air pressure control device, data acquisition device and soil sample placing device. The experimental confining pressure is set to 100 kPa, and the matric suction is set to 20, 50 and 80 kPa. The whole experiment process can be described as the following steps.

1. *Soil sample preparation* the collected Malan loess is crushed and then dried at 105 °C. The dried Malan loess is screened with 2 mm. Second, the water content of the Malan loess is set to 16%, and static compaction is applied for 24 h to make the water diffuse evenly in the loess. Finally, several soil samples with a size of 68 mm × 100 mm and a density of 1.70 g/cm^3 are prepared by the stratified sampling method.

2. *Saturation* the soil samples are saturated by the vacuum saturation method before consolidation.
3. *Consolidation* the soil samples are consolidated in the drained condition with a confining pressure value of 100 kPa after loading the saturated soil samples into GDS instrument. The consolidation process is over when the volume change of drained water is less than 0.01 mm^3 per 2 h.
4. *Setting the matric suction value* The air pressures of the GDS instrument are set to 20, 50 and 80 kPa through the air pressure control device. Meanwhile, the pore water pressure is set to zero.
5. *Shearing* the axial deviatoric stress is controlled by a multi-stage loading method. The failure stress value of soil sample is estimated using the conventional tri-axial shear strength index. Then, the multi-stage loading processes are set to 4–6 stages with loading q values of 50, 100, 150, 175 and 200 kPa, respectively, for each matric suction value. In addition, the creep stability criterion under q loading of each stage is specified as that the accumulation deformation per hour is less than 0.01 mm and/or the loading time of each stage lasts at least 1440 min.
6. Data processing and analysing: The deformation of each sample at different loading times can be obtained when the creep test is finished. Then, the stress–strain–time curves of different matric suctions can be plotted through the Boltzmann superposition principle due to the hierarchical loading in the creep test. Furthermore, the stress–strain isochronal curves with different S can be plotted by selecting the strain values at different times. Finally, the parameters of creep model are solved and verified using those creep data.

3 Theory of the improved Burgers model

3.1 The Burgers model

The Burgers model (Fig. 3a) is composed of a Kelvin body, spring and dashpot element in series. This model possesses elastic deformation in the early loading stage while possessing viscous and plastic deformation in the later stage. In addition, the Burgers

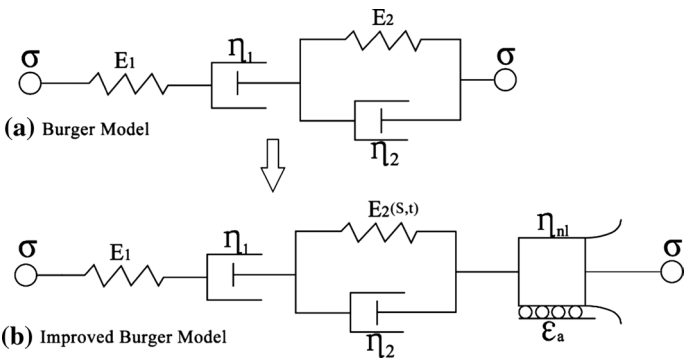

Fig. 3 The Burgers model (**a**) and the improved Burgers model (**b**)

model can describe the phenomenon of attenuation creep and constant-rate creep. The Burgers model is expressed as follows:

$$\sigma = \sigma_1 = \sigma_2 \tag{1}$$

$$\varepsilon = \varepsilon_1 + \varepsilon_2 \tag{2}$$

$$\sigma_1 = \sigma = E_1 \varepsilon_1 \tag{3}$$

$$\varepsilon = \frac{\sigma}{E_1} + \frac{\sigma}{\eta_1} + \frac{\sigma}{E_2}(1 - \exp\left(-\frac{E_2 t}{\eta_2}\right)) \tag{4}$$

where σ is the constant total stress; E_1, and E_2 are the viscoelastic moduli; η_1 and η_2 are the viscosity coefficient of the glue pot. σ_1 and σ_2 are the stress of the spring and Kelvin body, respectively; ε is the total strain; ε_1 and ε_2 are the strain of the spring and Kelvin body, respectively; t is time.

3.2 The improved Burgers model

There are some limitations in the Burgers model. It assumes that the creep behaviours are only caused by the deviatoric stress (q) without considering the effects of confining pressure, stress levels and matric suction. In addition, the Burgers model can only describe the attenuation creep and constant-rate creep stages. However, the actual creep failure processes of loess landslide include three stages of attenuation, constant-rate and acceleration. At present, some scholars have improved the Burgers model from different perspectives. For example, Jin and Ming (2016) proposed an improved Burgers model considering the influence of confining pressure on creep behaviours of coarse-grained soil; Ju et al. (2016) established a new Burgers model through studying the relationships of viscoelastic modulus with water content and time. In this study, the Burgers model is improved from two perspectives: (1) considering the influence of matric suction on the Burgers model and (2) considering the creep behaviours in the acceleration creep stage (Fig. 3b):

(1) A linear viscoelastic modulus is introduced to explain the influence of matric suction on creep behaviours in unsaturated loess. The changes of linear viscoelastic modulus along with the variation of matric suction can be studied according to the stress–strain isochronous curve. Therefore, when $\sigma \leq \sigma_s$, the Burgers model can be improved according to the following formulas:

$$\sigma = \sigma_1 = \sigma_2 \tag{5}$$

$$\varepsilon = \varepsilon_1 + \varepsilon_2 \tag{6}$$

$$\sigma_1 = \sigma = E_1 \varepsilon_1 \tag{7}$$

$$\sigma_2 = \sigma = E_2(S, t)\varepsilon_2 + \eta_2 \varepsilon_2. \tag{8}$$

The corresponding creep equation is as follows:

$$\varepsilon = \frac{\sigma}{E_1} + \frac{\sigma}{\eta_1} + \frac{\sigma}{E_2(S,t)}\left[1 - \exp\left(-\frac{E_2(S,t)t}{\eta_2}\right)\right] \tag{9}$$

where $E_2(S,t)$ is the expression revealing the relationship between the viscoelastic modulus, matric suction and time; S is the matric suction, and σ_s is the yield stress. The viscoelastic modulus and matric suction at different times are fitted by the linear formula $E_2 = PS + Q$ as follows:

$$P = a\ln(t) + b \tag{10}$$

$$Q = ct^d \tag{11}$$

where a, b, c, d are the fitting parameters. Hence, the relationships between the viscoelastic modulus and S can be obtained as follows:

$$E_2(S,t) = (a\ln(t) + b)S + ct^d. \tag{12}$$

The creep equation of the improved Burgers model can be obtained by substituting Eq. (12) into Eq. (3) and Eq. (9). When $\sigma \le \sigma_s$, then:

$$\varepsilon = \frac{\sigma}{E_1} + \frac{\sigma}{\eta_1} + \frac{\sigma}{(a\ln(t) + b)S + ct^d}\left[1 - \exp\left(-\frac{((a\ln(t) + b)S + ct^d)t}{\eta_2}\right)\right]. \tag{13}$$

(2) Improvement in the acceleration creep stage

When the creep stress is greater than the yield stress of loess, the nonlinear dashpot element with a strain trigger is applied to describe the soil deformation in the acceleration creep stage to improve the traditional Burgers model as follows:

$$\begin{aligned} \sigma &= \eta_{nl}\dot{\varepsilon}_{nl} \quad (\varepsilon \ge \varepsilon_a) \\ \varepsilon_{nl} &= 0 \quad (\varepsilon < \varepsilon_a) \end{aligned} \tag{14}$$

where ε_a is the strain value corresponding to soil samples entering into the accelerating creep stage. $\dot{\varepsilon}_{nl}$ is the viscosity coefficient of the nonlinear dashpot element. When $\varepsilon > \varepsilon_a$, the total stress of the soil sample is greater than the yield stress; then, the creep behaviour of soil sample enters the accelerating deformation stage, and the nonlinear dashpot element begins to be triggered:

$$\sigma = \sigma_1 = \sigma_2 = \sigma_3 \tag{15}$$

$$\varepsilon = \varepsilon_1 + \varepsilon_2 + \varepsilon_3 \tag{16}$$

$$\sigma_1 = \sigma = E_1\varepsilon_1 \tag{17}$$

$$\sigma_2 = \sigma = E_2(s,t)\varepsilon_2 + \eta_2\varepsilon_2 \tag{18}$$

$$\sigma_3 = \eta_{nl}\varepsilon_{nl} \tag{19}$$

where σ_3 is the nonlinear dashpot stress and ε_3 is the nonlinear dashpot strain. The corresponding creep equation can be described as follows:

$$\varepsilon = \frac{\sigma}{E_1} + \frac{\sigma}{\eta_1} + \frac{\sigma}{E_2(S,t)}\left[1 - \exp\left(-\frac{E_2(S,t)t}{\eta_2}\right)\right] + \frac{\sigma}{2\eta_{nl}}(t - t_0) \quad (20)$$

where t_0 is the time when soil sample enters into the accelerating creep stage. When $\varepsilon > \varepsilon_a$, then:

$$\varepsilon = \frac{\sigma}{E_1} + \frac{\sigma}{\eta_1} + \frac{\sigma}{(a\ln(t) + b)S + ct^d}\left[1 - \exp\left(-\frac{((a\ln(t) + b)S + ct^d)t}{\eta_2}\right)\right] + \frac{\sigma}{2\eta_{nl}}(t - t_0). \quad (21)$$

4 Experimental results

4.1 Strain–time curves analysis

The creep experiment results under the multi-stage loading conditions are shown in Table 2. The strain values at 1 min, 5 min, 10 min, 30 min, 60 min and 1440 min under each q loading condition are recorded. In addition, the stress–strain–time curves (Fig. 4) under different matric suction conditions can be plotted by using the Boltzmann superposition principle to process the experimental data (Rabotnov 1963). The creep deformation features of soil samples under different matric suction conditions are revealed in Fig. 4.

1. Figure 4 shows that a certain amount of instantaneous strain is generated in soil samples when a load is applied in each stage. Furthermore, the higher the stress level is, the greater the instantaneous strain is.
2. Figure 4 also shows that the creep strain–time curves of soil samples can be classified as three types. (1) When the q is less than or equal to 150 kPa, the strain–time curve tends to reach a steady state within a short time after the instantaneous strain, and the soil samples exhibit the behaviour of decaying creep. (2) When the q is 175 kPa, the creep curve exhibits acceleration creep deformation with a gradually increasing creep

Table 2 The results of creep experiments under different matric suction conditions

Simple number	*S*/ kPa	*q* / kPa	Strain/1 min	Strain/5 min	Strain/10 min	Strain/30 min	Strain/60 min	Strain/1440 min
1	20	25	0.047	0.692	0.872	0.892	0.897	0.920
		50	0.974	1.007	1.025	1.064	1.095	1.157
		100	1.417	1.926	2.007	2.115	2.174	2.329
		150	2.571	3.758	4.111	4.438	4.599	4.844
		175	4.881	4.929	5.008	6.557	9.617	12.190
		200	12.215	12.237	12.252	12.433	20.294	–
2	50	50	0.262	0.797	0.816	0.838	0.851	0.955
		100	1.180	1.604	1.703	1.836	1.881	2.064
		150	2.289	3.584	4.259	5.038	5.352	5.710
		175	5.964	7.269	8.898	11.465	24.910	–
3	80	50	0.599	2.010	2.357	2.394	2.410	2.471
		100	2.754	3.437	3.540	3.624	3.671	3.801
		150	3.985	5.206	5.609	5.919	6.038	6.212
		175	6.268	6.332	6.413	7.281	7.989	8.757
		200	8.797	8.827	8.858	9.976	19.545	–

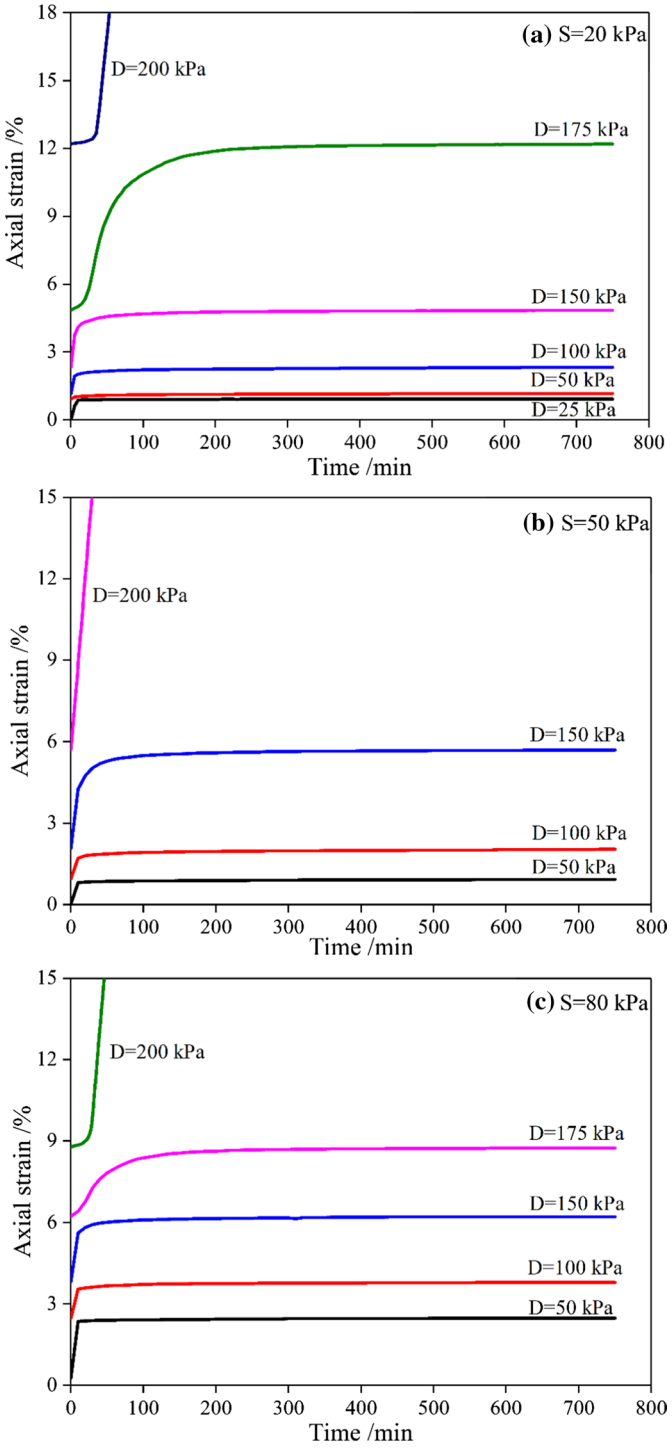

Fig. 4 Strain–time curves of soil samples under different matric suctions: **a** $S=20$ kPa, **b** $S=50$ kPa, **c** $S=80$ kPa,

rate after the instantaneous strain and then tends to show attenuation creep deformation until the creep is stable. (3) When q is 200 kPa, the creep curve has a steep increase and enters the acceleration creep stage; the creep rate becomes larger until the soil samples fail. The duration of this stage is short, and this stage is characterized by an up-warping section in the creep curve.

3. Under the condition of the same loading stress level, the larger the matric suction is, the smaller the initial strain is when the creep deformation enters the accelerated creep stage. In addition, Table 2 shows that there is a steady creep stage with constant strain velocity before the creep behaviour of soil sample enters to acceleration creep stage.

4.2 Stress–strain isochronal curve

The strain–time curves under the conditions of different matric suctions are shown in Fig. 4. The strain values at the times of 1 min, 5 min, 10 min, 20 min, 30 min, 60 min, 100 min and 360 min under each loading condition are selected from Fig. 4 to obtain the stress–strain isochronal curves with different matric suctions (Fig. 5).

1. Figure 5 shows that the stress–strain isochronal curves are all clusters of curves under the conditions of different matric suction values, and the curves gradually become concave to the strain axis along with the increase in stress and time. These phenomena indicate that the Malan loess has obvious nonlinear creep behaviours. Moreover, the greater the deviatoric stress level and the longer the deformation time are, the greater the degree of concavity to the strain axis is, which indicates that the nonlinear degree increases along with the increase in the deviatoric stress level and time.
2. Figure 5a shows that, when the matric suction is 20 kPa and q is less than 150 kPa, the stress–strain isochronal curves of the soil sample exhibit nearly linear features, and the soil sample exhibits the feature of linear viscoelasticity. In addition, the corresponding creep process is gradually attenuated to be steady state. When the q is greater than 150 kPa, the stress–strain curve is nonlinear and the soil sample shows the characteristic of nonlinear viscoplasticity. In addition, the corresponding creep deformation increases with increasing time, indicating an unstable deformation process. Similar results are also shown in Fig. 5b, c.

Figure 6 suggests that matric suction has a significant impact on the creep behaviours of Malan loess under the same confining pressures and stress level conditions. Furthermore, the larger the matric suction is, the greater the strain is when the creep deformation of soil sample reaches steady state. When the confining pressure is 100 kPa and q is 150 kPa, the creep strains at steady state are 4.84%, 5.69% and 6.22% corresponding to S of 20, 50 and 80 kPa, respectively.

4.3 Variation of long-term strength under different matric suctions

The long-term strengths of soil samples under different matric suctions can be obtained based on the stress–strain isochronal curves (Fig. 5). The long-term strengths with matric suction of 20 kPa, 50 kPa and 80 kPa are 151, 159 and 168 kPa, respectively. The long-term strength of Malan loess increases along with the increase in matric suction.

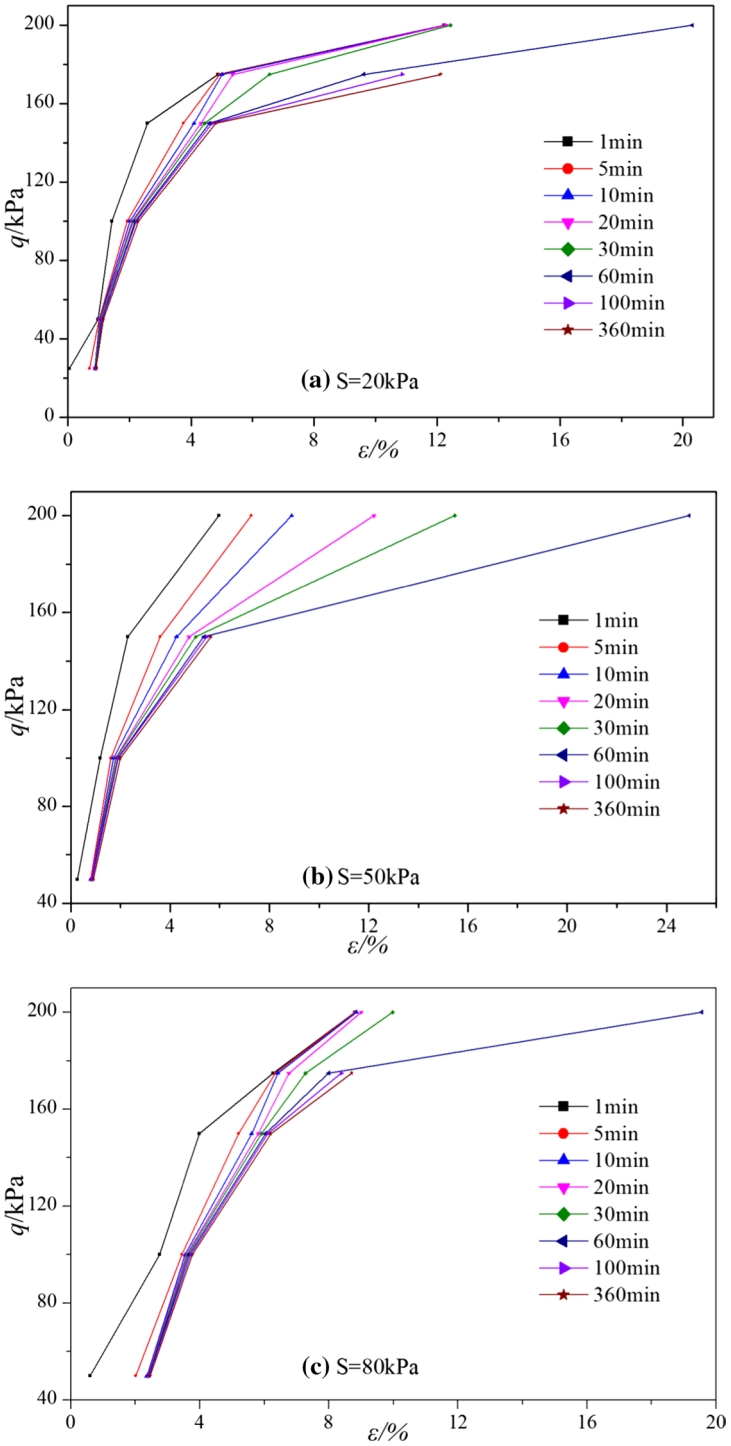

Fig. 5 Stress–strain isochronal curves of soil samples under different matric suctions: **a** $S=20$ kPa, **b** $S=50$ kPa, **c** $S=80$ kPa

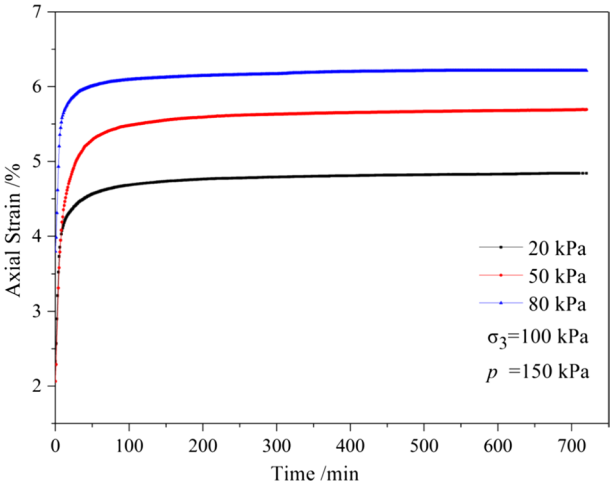

Fig. 6 Strain–time curves under different matric suctions ($\sigma_3 = 100$ kPa, $p = 150$ kPa)

5 Solution and verification of the improved Burgers model

5.1 Variation of the linear viscoelastic modulus under different matric suctions

According to the stress–strain isochronal curves of soil samples (Fig. 5), the variation of linear viscoelastic modulus under different matric suctions is studied, and then, viscoelastic modulus values for different matric suctions and times can be calculated (Table 3). Table 3 suggests that viscoelastic modulus gradually decreases with increasing time under same S condition.

5.2 Solution and verification of model parameters

Figure 7 shows that the viscoelastic modulus values of soil samples have a linear relationship with the matric suction at the same time. Hence, the linear formula $E_2 = PS + Q$ is used to fit the relationships between viscoelastic modulus and matric suction at different times (Fig. 7). The parameters P and Q are obtained according to the fitting formula (Table 4).

The fitting equations in which the parameters P and Q vary along with the changes of time are obtained based on Eqs. (10) and (11) and the data in Table 4. The obtained equations are $P = 0.0246 \ln(t) - 0.565$ and $Q = 80.886t^{-0.045}$, respectively, with corresponding R^2 values of 0.988 and 0.970. There is a great linear relationship between the viscoelastic

Table 3 Linear viscoelastic modulus values of loess with different matric suctions

20 kPa	Time/min	5	20	30	60	100	200	360	720
	Viscoelastic modulus/(10^3 kPa)	62.32	57.65	56.47	54.56	53.30	52.30	51.53	49.83
50 kPa	Time/min	5	20	30	60	100	200	360	720
	Viscoelastic modulus/(10^3 kPa)	58.71	51.35	50.12	48.56	47.38	46.41	46.06	45.2
80 kPa	Time/min	5	20	30	60	100	200	360	520
	Viscoelastic modulus/(10^3 kPa)	36.12	28.27	27.53	26.74	26.45	26.25	26.01	25.96

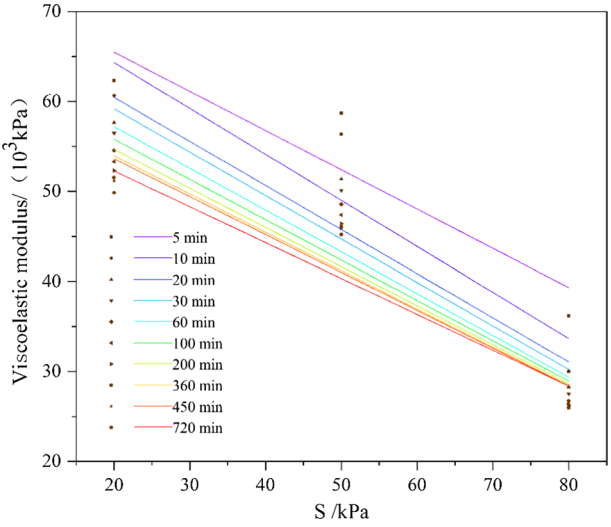

Fig. 7 Relationship between viscoelastic modulus and matric suction

Table 4 The fitting results of the viscoelastic modulus with matric suction

Time (min)	P	Q	R^2	Time (min)	P	Q	R^2
5	−0.5359	74.196	0.851	100	−0.4457	64.752	0.906
10	−0.5108	74.545	0.853	200	−0.4343	63.366	0.909
20	−0.4896	70.236	0.902	360	−0.4253	62.468	0.902
30	−0.4824	68.828	0.905	450	−0.4203	62.018	0.900
60	−0.4637	66.468	0.903	720	−0.3978	60.221	0.889

modulus and matric suction. Therefore, the creep equation of Malan loess can be expressed as follows:

when $\sigma \le \sigma_s$, then:

$$\varepsilon = \frac{\sigma}{E_1} + \frac{\sigma}{\eta_1} + \frac{\sigma}{(0.0246\ln(t) - 0.565)S + 80.886t^{-0.045}} \cdot \left[1 - \exp(-\frac{((0.0246\ln(t) - 0.565)S + 80.886t^{-0.045})t}{\eta_2}\right] \tag{22}$$

when $\varepsilon > \varepsilon_a$, then:

$$\varepsilon = \frac{\sigma}{E_1} + \frac{\sigma}{\eta_1} + \frac{\sigma}{(0.0246\ln(t) - 0.565)S + 80.886t^{-0.045}} \cdot \left[1 - \exp(-\frac{((0.0246\ln(t) - 0.565)S + 80.886t^{-0.045})t}{\eta_2}\right] + \frac{\sigma}{2\eta_{nl}}(t - t_0) \tag{23}$$

Next, it is necessary to solve the relevant parameters of the improved creep model. In this study, relevant parameters are solved by adopting the BFGS algorithm and general global optimization method to fit the strain–time curves in the mathematical software 1stOpt. These parameters are listed in Table 5. Then, the fitted strain–time curves are

Table 5 Parameters of the improved Burgers model

Matric suction	q (kPa)	$E_1(10^3$ kPa)	$\eta_1(10^3$ kPa min)	$\eta_2(10^3$ kPa min)	$\eta_{nl}(10^3$ kPa min)	R^2
20 kPa	25	106.898	112.155	0.391	501.791	0.652
	50	44.119	584.597	0.987		0.991
	100	38.891	598.868	2.808		0.985
	150	32.374	629.713	1.455		0.917
	175	17.951	69.639	2.983		0.899
	200	11.649	74.458	141.483		0.934
50 kPa	50	91.315	124.929	4.374	495.149	0.999
	100	40.664	143.587	1.556		0.982
	150	35.660	90.6308	3.651		0.870
	200	7.0384	37.5461	0.181		0.999
80 kPa	50	63.457	29.5875	0.762	393.327	0.998
	100	46.297	60.2024	0.934		0.983
	150	76.182	33.0856	4.754		0.994
	175	39.044	40.8286	0.548		0.882
	200	16.178	73.6843	0.2146		0.952

analysed and compared with the experimental strain–time curves. Figure 8 shows that the improved Burgers model fits the strain–time curves well, which can accurately reflect the magnitude relationship of creep strain considering matric suction in unsaturated loess and can further comprehensively and accurately reflect the whole process of unsaturated loess creep.

6 Discussion

6.1 Effects of matric suction on landslide instability

In this study, the tri-axial creep tests are performed on Malan loess specimens under different matric suctions, namely 20, 50 and 80 kPa, respectively. It can be concluded that the creep properties of Malan loess are also closely related to the matric suction, although the effects of water content, confining pressure, soil particle composition and other factors on creep behaviours have been studied (Gao et al. 2012). In addition, it is revealed that the matric suction plays an important role in the stability of loess landslide. Hence, the results of this study are significant for exploring the landslide instability mechanism.

6.2 Creep behaviours of Malan loess

In general, the loess creep behaviours under different conditions exhibit different features. For example, Long et al. (2010) had pointed that the loess creep deformation included constant-rate creep, accumulation creep and creep failure stages under the effect of water contents. Wang et al. (2020) had deciphered the loess creep behaviours using multi-loading tri-axial creep tests under different water contents and revealed the relationships among the creep rate at the steady-state creep stage, the initial strain and initial shear modulus.

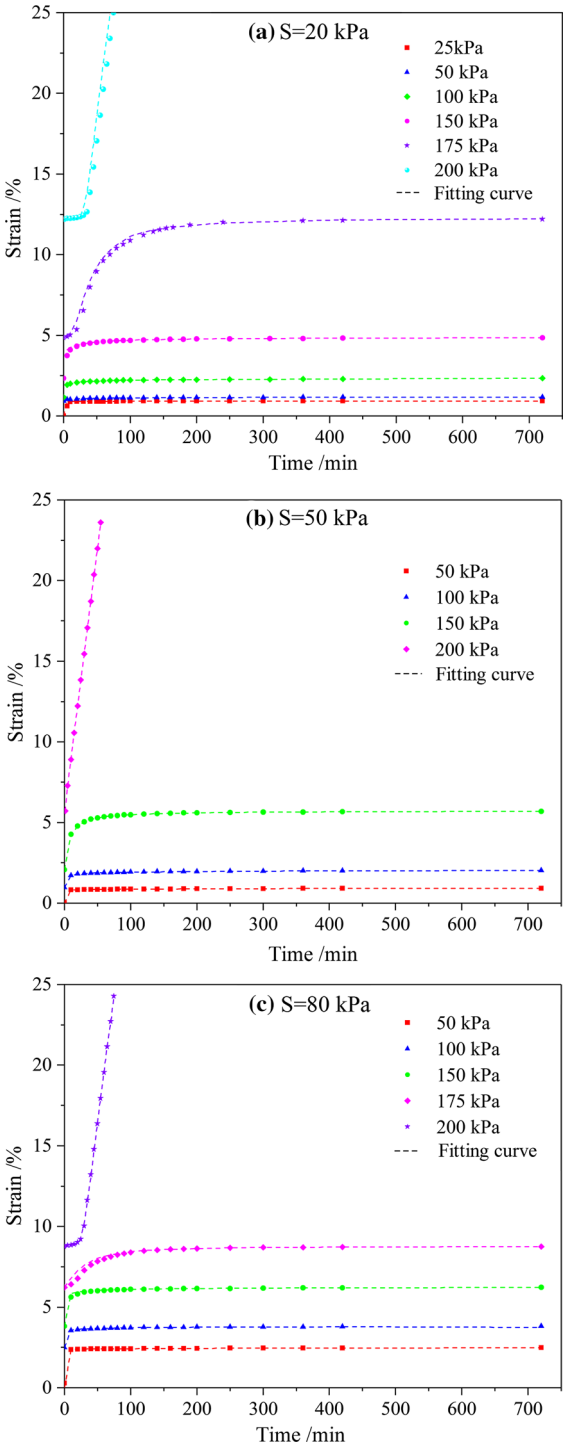

Fig. 8 Comparison of experiment curves and fitting curves under different matric suctions: **a** $S=20$ kPa, **b** $S=$d0 kPa, **c** $S=80$ kPa,

Guo et al. (2015) had studied the creep properties of remoulded loess under different water contents and confining pressures. In this study, the creep behaviours of Malan loess exhibit viscoelastic and viscoplastic creep properties and have attenuation creep, constant-rate creep and accumulation creep stages. In addition, it can also be revealed that the loess from different places exhibit different creep behaviours due to the difference of particle concentration, loess structure and sedimentary environment.

6.3 Discussions of improved Burgers model

Although some empirical creep models and Burgers models considering different factors have been proposed to implement an in-depth study of soil creep behaviour, the matric suction is rarely considered and the accelerated creep stage of creep deformation is rarely reflected in the existing studies. Therefore, an improved Burgers model is established considering the matric suction factor and accelerated creep deformation as well as combining this with tri-axial creep experimental data based on the Burgers model. Figure 8 suggests that the improved Burgers model has good accuracy and can effectively reflect the creep features of unsaturated Malan loess.

Furthermore, some deficiencies still exist in the improved Burgers model. On one hand, the conclusions of this paper are based on the results of creep tests; it is inevitable to have some limitations due to the small number of soil samples. On the other hand, due to the formation and evolution of landslides depend on the effects of some factors such as matric suction and water content of soil, rainfall, groundwater and human activities, it is difficult for the improved Burgers model to take all of these complex factors into account.

To better link the creep test results and improved Burgers model with the mechanism of loess landslides, the improved Burgers model should be incorporated into a numerical simulation program as a new module, which can better make use of the field monitoring data and the proposed creep model to analyse the landslide processes. Based on the finding of this study, the evolutional processes of the landslide under different matric suctions can be analysed and predicted.

7 Conclusion

In this study, the creep behaviours of Malan loess are studied based on a series of tri-axial undrained creep tests. Then, an improved Burgers model considering the effects of matric suction values is proposed. Some conclusions can be drawn as follows.

1. The Malan loess has strong creep behaviour. When the deviatoric stress is less than the yield stress, the soil sample exhibits a linear viscoelasticity. When the deviatoric stress is greater than the yield stress, the soil sample exhibits a nonlinear viscoelasticity.
2. The long-term strength of Malan loess increases along with the increase in matric suction. The viscoelastic modulus decreases with the increase in time under the same matric suction condition. At the same time, under the condition of the same loading stress level, the larger the matric suction, the smaller the initial strain when the creep deformation enters the acceleration creep stage. In addition, the relationship between the viscoelastic modulus and matric suction is linear.
3. A stress–suction–strain–time model (the improved Burgers model) which is suitable for Malan loess is established by connecting a nonlinear dashpot element in series with

the Burgers model and combining the functional relationship between the viscoelastic modulus and matric suction. It can be concluded that the improved Burgers model can more accurately describe the creep behaviours of unsaturated Malan loess under the conditions of different matric suctions by comparing the modelling results to the testing results.

Acknowledgements This research is funded by the Natural Science Foundation of China (No. 41807285, 41972280 and 51679117), the National Science Foundation of Jiangxi Province, China (NO. 20192BAB216034), the China Postdoctoral Science Foundation (NO. 2019M652287) and the Jiangxi Provincial Postdoctoral Science Foundation (NO. 2019KY08).

References

Bhat DR, Bhandary NP, Yatabe R (2013) Residual-state creep behavior of typical clayey soils. Nat Hazards 69(3):2161–2178

Chen HX, Zhang LM, Chang DS, Zhang S (2012) Mechanisms and runout characteristics of the rainfall-triggered debris flow in Xiaojiagou in Sichuan province, China. Nat Hazards 62(3):1037–1057

Fan X, Xu Q, Scaringi G, Li S, Peng D (2017) A chemo-mechanical insight into the failure mechanism of frequently occurred landslides in the Loess Plateau, Gansu Province, China. Eng Geol 228:337–345. https://doi.org/10.1016/j.enggeo.2017.09.003

Fredlund DG, Xing A, Fredlund MD, Barbour SL (1995) The relationship of the unsaturated soil shear to the soil-water characteristic curve. Can Geotech J 32(3):440–448

Gallage C, Uchimura T (2016) Direct shear testing on unsaturated silty soils to investigate the effects of drying and wetting on shear strength parameters at low suction. J Geotech Geoenviron Eng 142(3):04015081. https://doi.org/10.1061/(asce)gt.1943-5606.0001416

Gao H, Chen Y, Liu H, Liu J, Chu J (2012) Creep behavior of eps composite soil. Sci China Technol Sci 55(11):3070–3080. https://doi.org/10.1007/s11431-012-4967-6

Graham J, Tanaka N, Crilly T, Alfaro M (2001) Modified cam-clay modelling of temperature effects in clays. Can Geotech J 38(3):608–621. https://doi.org/10.1139/t00-125

Guo H, Luo Y, Wang P (2015) Research on triaxial creep characteristics and models of remolded loess under respective and graded loading. Rock Soil Mech 36(6):1627–1632

Hou X, Vanapalli SK, Li T (2018) Water infiltration characteristics in loess associated with irrigation activities and its influence on the slope stability in Heifangtai Loess Highland, China. Eng Geol 234:27–37. https://doi.org/10.1016/j.enggeo.2017.12.020

Huang M, Liu XR, Zhu YH, Zhong ZL (2009) A study of behaviors of generalized kelvin-voigt model under low frequency cyclic load. Rock Soil Mech 30(8):2300–2304

Huang F, Yin K, Huang J, Gui L, Wang P (2017) Landslide susceptibility mapping based on self-organizing-map network and extreme learning machine. Eng Geol 223:11–22

Jeong S, Lee K, Kim J, Kim Y (2017) Analysis of rainfall-induced landslide on unsaturated soil slopes. Sustain Basel 9(7):1280. https://doi.org/10.3390/su9071280

Jin DH, Ming XU (2016) Parameter correction method of burgers model for coarse-grained soil considering confining pressure. Eng Mech 033(012):135–142

Ju N, Huang H, Zheng D, Zhou X (2016) Improved burgers model for creep characteristics of red bed mudstone considering water content. Rock Soil Mech 37(S2):67–74

Lai X, Wang S, Qin H, Liu X (2010) Unsaturated creep tests and empirical models for sliding zone soils of qianjiangping landslide in the three gorges. J Rock Mech Geotech Eng. 2:57–62

Lai XL, Wei-Min YE, Wang SM (2012) Experimental study on unsaturated creep characteristics of landslide soils. Chin J Geotech Eng 34(2):286–293

Lee ML, Ng KY, Huang YF, Li WC (2014) Rainfall-induced landslides in Hulu Kelang area, Malaysia. Nat Hazards 70(1):353–375

Li D-W, Fan J-H, Wang R-H (2011) Research on visco-elastic-plastic creep model of artificially frozen soil under high confining pressures. Cold Reg Sci Technol 65(2):219–225. https://doi.org/10.1016/j.coldregions.2010.08.006

Ling X, Dai F, Tu X, Tham LG, Zhou Y, Iqbal J (2014) Landslides in a loess platform, North-West China. Landslides 11(6):993–1005

Liu MD, Carter JP (2002) A structured cam clay model. Can Geotech J 39(6):1313–1332. https://doi.org/10.1139/t02-069
Long J, Guo W, Li P, Li T (2010) Creep property of soil in sliding zone of loess landslide Yantu Gongcheng Xuebao/Chin J. Geotech Eng 32(7):1023–1028
Mahmood K, Kim JM, AshrafZiaurrehman M (2016) The effect of soil type on matric suction and stability of unsaturated slope under uniform rainfall. Ksce J Civ Eng 20(4):1294–1299
Nguyen ST, Dormieux L, Pape YL, Sanahuja J (2011) A burger model for the effective behavior of a micro-cracked viscoelastic solid. Int J Damage Mech 20(8):1116–1129
Qiu J, Wang X, Lai J, Zhang Q, Wang J (2018) Response characteristics and preventions for seismic subsidence of loess in northwest china. Nat Hazards 92(3):1909–1935
Rabotnov YN (1963) On the equation of state of creep. ARCHIVE: Proceedings of the institution of mechanical engineers, Conference proceedings 1964–1970 (vols 178–184), Various titles labelled Volumes A to S 178(31):117–122
Sivasithamparam N, Karstunen M, Bonnier P (2015) Modelling creep behaviour of anisotropic soft soils. Comput Geotech 69:46–57
Song Y-S, Chae B-G, Lee J (2016) A method for evaluating the stability of an unsaturated slope in natural terrain during rainfall. Eng Geol 210:84–92. https://doi.org/10.1016/j.enggeo.2016.06.007
Tang M, Xu Q, Huang R (2014) Site monitoring of suction and temporary pore water pressure in an ancient landslide in the three gorges reservoir area, China. Environ Earth Sci 73(9):5601–5609. https://doi.org/10.1007/s12665-014-3814-4
Wan LH, Cao P, Huang YH, Wang YX, Zhang XY (2011) Creep test of hard rock and modified generalized Kelvin creep model. Appl Mech Mater 90–93:626–632
Wang ZC, Qiao LP (2011) A review and discussion on creep behavior of soil and its models. Rock Soil Mech 32(8):2251–2260
Wang J-J, Liang Y, Zhang H-P, Wu Y, Lin X (2013) A loess landslide induced by excavation and rainfall. Landslides 11(1):141–152. https://doi.org/10.1007/s10346-013-0418-0
Wang X, Wang J, Zhan H, Li P, Qiu H, Hu S (2020) Moisture content effect on the creep behavior of loess for the catastrophic baqiao landslide. CATENA. https://doi.org/10.1016/j.catena.2019.104371
Xie X, Shengwen Q, Zhao F, Wang D (2018) Creep behavior and the microstructural evolution of loess-like soil from xi\"an area, china. China Eng Geol 236:43–59
Xu L, Meng X, Xu X (2014) Natural hazard chain research in china: a review. Nat Hazards 70(2):1631–1659
Xu X-Z, Guo W-Z, Liu Y-K, Ma J-Z, Wang W-L, Zhang H-W, Gao H (2017) Landslides on the loess plateau of china: a latest statistics together with a close look. Nat Hazards 86(3):1393–1403
Xu Y, Leung CF, Yu J, Chen W (2018) Numerical modelling of hydro-mechanical behaviour of ground settlement due to rising water table in loess. Nat Hazards 94(1):241–260
Yang Y, Lai Y, Chang X (2010) Experimental and theoretical studies on the creep behavior of warm ice-rich frozen sand. Cold Regions Sci Technol. 63(1–2):0–67
Yuliza E, Habil H, Munir MM, Irsyam M, Abdullah M, Khairurrijal. (2016) Study of soil moisture sensor for landslide early warning system: Experiment in laboratory scale. J Phys Conf Ser 739:012034. https://doi.org/10.1088/1742-6596/739/1/012034
Zhang M, Liu J (2009) Controlling factors of loess landslides in western china. Environ Earth Sci 59(8):1671–1680. https://doi.org/10.1007/s12665-009-0149-7
Zhang D, Wang G (2007) Study of the 1920 haiyuan earthquake-induced landslides in loess (China). Eng Geol 94(1):76–88
Zhao X, Zhou G (2013) Experimental study on the creep behavior of frozen clay with thermal gradient. Cold Reg Sci Technol 86:127–132. https://doi.org/10.1016/j.coldregions.2012.10.012
Zhao Y-l, Cao P, Wang W-J, Wan W, Liu Y-K (2009) Viscoelasto-plastic rheological experiment under circular increment step load and unload and nonlinear creep model of soft rocks. J Central South Univ Technol 16(3):488–494
Zhou J, Tang Y, Yang P, Zhang X, Zhou N, Wang J (2012) Inference of creep mechanism in underground soil loss of karst conduits i Conceptual model. Nat Hazards 62(3):1191–1215
Zhu Y-b, Yu H-m (2014) An improved mesri creep model for unsaturated weak intercalated soils. J Central South Univ 21(12):4677–4681. https://doi.org/10.1007/s11771-014-2476-4
Zhuang J, Peng J, Xu C, Li Z, Densmore A, Milledge D, Iqbal J, Cui Y (2018) Distribution and characteristics of loess landslides triggered by the 1920 haiyuan earthquake, northwest of china. Geomorphology 314:1–12. https://doi.org/10.1016/j.geomorph.2018.04.012